Pergamon

Geochimica et Cosmochimica Acta, Vol. 67, No. 7, pp. 1289–1304, 2003

0016-7037/03 $30.00 + .00

doi:10.1016/S0016-7037(02)01270-X

Forces and ionic transport between mica surfaces: Implications for pressure solution

NORMA ALCANTAR,[1] JACOB ISRAELACHVILI,[1,*] and JIM BOLES[2]

[1]Department of Chemical Engineering, University of California, Santa Barbara, CA 93106, USA
[2]Department of Geological Sciences, University of California, Santa Barbara, CA 93106, USA

(*Received May* 28, 2002; *accepted in revised form September* 25, 2002)

Abstract—Using a surface forces apparatus (SFA), we have studied the interactions between mica surfaces in pure and mixed NaCl and $CaCl_2$ solutions at relevant geological conditions of pressure and electrolyte composition. Our results show that the short-range (0–50 Å) colloidal forces, including attractive van der Waals and ion-correlation forces, repulsive electrostatic forces, and oscillatory or monotonically repulsive hydration (surface-induced water structure-dependent) forces are involved in different stages of pressure solution. These forces depend on the type (Na^+, Ca^{2+}, and H^+) and concentration (6–600 mM) of the cations present in the solution. Equilibrium water film thicknesses were measured as a function of the applied (normal) pressure up to 50 MPa (500 atm) and ranged from 30 to 0 Å at pressures above 10 MPa (100 atm). Measurements were also made of the rates of diffusion and exchange of ions into and out of such ultrathin films, and on the nucleation and growth of ionic crystallites on and between the surfaces, which occurred only in the presence of calcium ions. Diffusion of ions into and out of structured water films as thin as one to five water molecules (3 to 15 Å) were found to be surprisingly rapid and never less than two orders of magnitude below the diffusion in bulk water. In contrast, the rates of binding and exchange of ions to the surfaces were found to be the rate-limiting steps to adsorption and crystal formation. These findings imply that, for certain systems or conditions, pressure solution rates could be limited by surface reactions rather than by ion diffusion in thin fluid films.

1. INTRODUCTION AND BACKGROUND

1.1. Current Issues in Pressure Solution

Pressure solution is the preferential dissolution of minerals along stressed grain boundaries resulting in the interpenetration (suturing) of grains and, on a larger scale, the development of stylolites (see extensive review by Tada et al., 1987). Geologic studies of pressure solution have noted the almost ubiquitous occurrence of clays along stylolitic seams at the outcrop scale, and petrologic studies have also noted that the presence of mica enhances quartz dissolution (Heald, 1955; Houseknecht, 1987). Recently, Bjørkum (1996) reported that quartz grains had dissolved around mica flakes without deformation of the mica, suggesting that the role of pressure only serves to keep the grains together.

Little is known at the submicroscopic and molecular levels about fluid-filled interfaces between dissimilar minerals, although there are considerable data on mineral surfaces in free solution (Hochella, 1995). The role of clays in pressure solution, including what kind of clays are involved and the nature of their interaction with thin fluid films, is still not well understood. The general explanation is that diffusion is enhanced due to the increased water film thickness associated with clay surfaces (Renard et al., 1997). Different stages of pressure solution are believed to involve ion dissolution, diffusion (transport), ion binding or exchange, and precipitation, although some of these stages are obviously related or occur simultaneously.

Currently, three models of quartz pressure solution are proposed (den Brok, 1998; Renard et al., 1999) and although the models do not specifically address the role of clay, a main difference between the models is the thickness of the water film and the path length through which material must diffuse (Figure 1). The models assume that if the water film becomes very thin, its molecular-scale structuring will limit diffusion rates. In the three models, the deformation rate (i.e., material transport rate) varies considerably depending on the assumed diffusion rates in the thin water films and the presence of channels.

The three models, following den Brok's nomenclature (den Brok, 1998), are the **thin-film**, the **grain-boundary** (Gratz, 1991), and the island-channel model. The thin-film model (Weyl, 1959; Rutter, 1983; Kruzhanov and Stöckhert, 1998) assumes two quartz grains are separated by a film of structured water a few nanometers thick. Mass is transferred from the quartz grains along the film and pressure solution is relatively slow due to the low diffusion rate in the water. The Gratz **grain-boundary** model (Gratz, 1991; den Brok, 1998) considers stress corrosion micro-cracks that can occur along the grain boundary or at the margin of contacts. The cracks, which cause enhanced diffusion, are continuously extended by stress corrosion at the crack tips, maintaining a plumbing network to the grain boundary. In this model, material diffuses from the thin fluid film between the rather narrow "islands" of quartz into the relatively large channels being maintained by microcracks, plastic deformation and free face pressure solution (Tada et al., 1987). In the **island-channel** model (Raj, 1982; Cox and Patterson, 1991; Lehner, 1995; Spiers and Schutjens, 1995) stress is transmitted across solid "island" quartz–quartz contacts and material diffuses through relatively large (nanometer to micrometer scale) adjacent channels. The islands and channels continuously move but the overall configuration is maintained. Models 2 and 3 fit geologic and experimental observations of pressure solution surfaces that show deep dissolution

* Author to whom correspondence should be addressed.

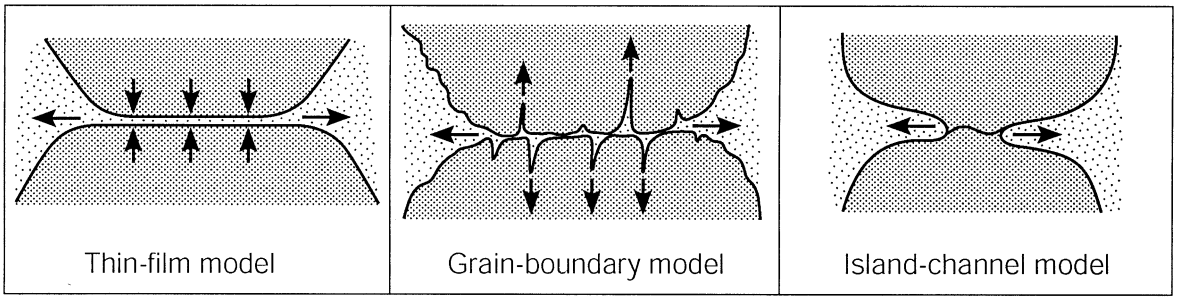

Fig. 1. Proposed mechanisms of pressure solution (after den Brok, 1998). Vertical arrows refer to pressures or crack propagation directions; horizontal arrows refer to silica transport.

pits (Pittman, 1974; Welton, 1984; den Brok, 1998). The deformation rate in these models is faster than in Model 1 due to the shorter diffusion path length. All of these models have in common an estimate of the diffusion coefficient in water, which varies according to the thickness of the fluid film.

Revil (1999) considered a model like Model 1, but he used a much higher fluid diffusivity in thin fluid films between quartz grains—one order lower than the bulk, based on the work of Vigil et al. (1994), in contrast to the five orders used by Rutter (1976). Revil postulates relatively open diffusion pathways between silica–silica surfaces, in part due to their unique steric repulsive interaction. Notably, Revil's model is also a closed system in which he considers local precipitation of silica at the scale of the representative elementary volume (Renard et al., 1999; Revil, 1999).

Our interest in this problem is focused on the role of mica in the pressure solution of quartz. Workers have generally attributed this to thicker water films associated with mica–quartz contacts (Renard et al., 1999), although measurements of such films between quartz and mica have not been made. We are studying mica–quartz interface interactions, including measurements of water film thickness, viscosity, and diffusion rates. Our initial work, described here, characterizes the mica–fluid–mica interface in close contact. This will provide a reference for subsequent work on the mica–fluid–silica interface. Our initial results suggest that even in the simple mica–fluid–mica system, geologically realistic fluid compositions plays an important but unexpected role in the behavior of the system, and that—in agreement with (Revil, 2001) but for different reasons—diffusion rates may not be as much of an issue as once thought.

1.2. Current Issues in the Short-Range Colloidal Forces Between Clay–Mineral Surfaces

Force-distance, *F(D),* measurements using the Surface Forces Apparatus technique have been applied to many different surfaces, including mica and silica, immersed in different electrolyte solutions (Israelachvili, 1991; Ducker et al., 1994; Vigil et al., 1994). In general, at surface separations greater than ~20 Å, measured forces have been in good agreement with theory—the so-called Derjaguin–Landau–Verwey–Overbeek (DLVO) theory of colloidal stability (Verwey and Overbeek, 1948), which includes the repulsive electrostatic "double-layer" force and attractive van der Waals force (Israelachvili, 1991). The DLVO theory is a nonspecific, continuum theory that does not take into consideration the discrete molecular nature of the surfaces, solvent, or ions, and other factors that can become important at small distances (Israelachvili, 1991). Between mica surfaces there is good agreement between theory and experiment at all separations down to contact (at $D = 0$) only in dilute electrolyte solutions—below 1 mM in 1:1 electrolytes such as NaCl, and below 0.1–1 M in 2:1 electrolytes such as $CaCl_2$ (Figure 2). In contrast, the measured forces between smooth but amorphous silica surfaces show deviations from DLVO behavior under all solution conditions, even in pure water (Vigil et al., 1994). These additional non-DLVO forces have been found to depend on the specific nature of the surfaces, the solvent, the ions in the solvent, and the ions adsorbed on the surfaces. In the case of interactions between clay and other mineral surfaces in aqueous solutions, these interactions can be attractive, repulsive and/or oscillatory, and they include the following (Figure 3):

(I) Monotonically repulsive forces between surfaces with protruding charged groups as occur on amorphous silica surfaces (Vigil et al., 1994), or surfaces having large co-ions (Frens and Overbeck, 1972) or large adsorbed counterions (Pashley, 1982). Protruding charges shift out the repulsive Outer Helmholtz Plane (OHP) relative to the attractive van der Waals plane.

(II) Monotonically repulsive "steric-hydration" forces between surfaces with a strongly bound layer of water molecules (van Olphen, 1977; Pashley, 1981; Viani et al., 1983; Pashley and Israelachvili, 1984; Christenson et al., 1987; Kjellander et al., 1988).

(III) "Oscillatory-hydration" forces due to solvent structuring into layers adjacent to smooth, crystalline surfaces. Oscillatory forces have a periodicity of the water molecule (about 2.7 Å) and have a range of about 15 Å (Christenson et al., 1982; Israelachvili and Pashley, 1983; Israelachvili and Wennerström, 1996). Their multiple adhesive minima give rise to the discrete "crystalline swelling" of clays (Caffrey and Bilderback, 1983; Quirk and Marcelja, 1997).

(IV) Attractive "ion correlation" forces in divalent counterion solutions such as $CaCl_2$ can give rise to a reduced double-layer repulsion or even a short-range attraction which originates from the van der Waals interaction between the

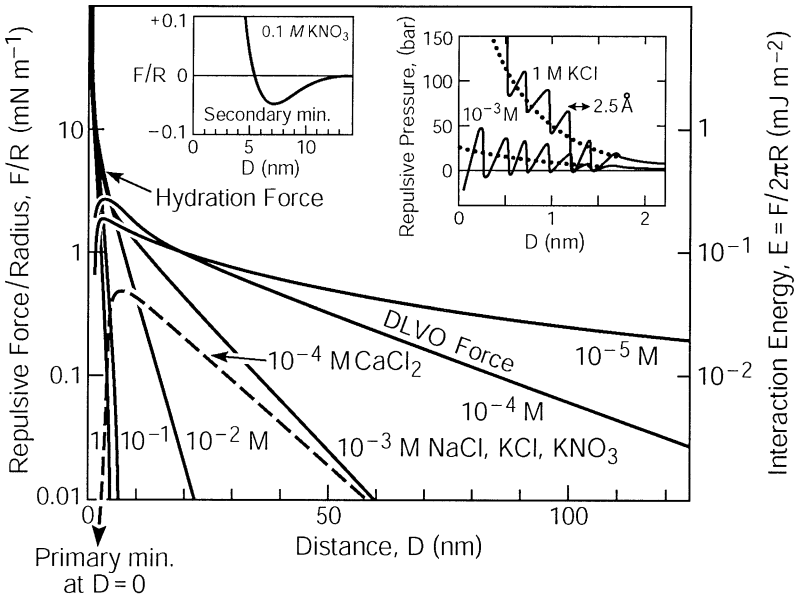

Fig. 2. Colloidal forces previously measured between two mica surfaces in pure monovalent (10^{-5} to 1 M NaCl, KCl, KNO_3) and divalent (10^{-4} M only $CaCl_2$) solutions (Pashley, 1981; Christenson et al., 1982; Israelachvili and Pashley, 1983; Pashley and Israelachvili, 1984; Christenson et al., 1987; Kjellander et al., 1988; McGuiggan and Israelachvili, 1990; Israelachvili, 1991; Israelachvili and Wennerström, 1996).

polarizable *counterions* of the two double-layers (van Olphen, 1977; Viani et al., 1983; Guldbrand et al., 1984; Kjellander et al., 1988; Kjellander et al., 1990; Kekicheff et al., 1993). Finite counterion size effects can also give rise to an additional "osmotic repulsion" at separations above one Debye length and to a "depletion attraction" at smaller separations (Paunov and Binks, 1999).

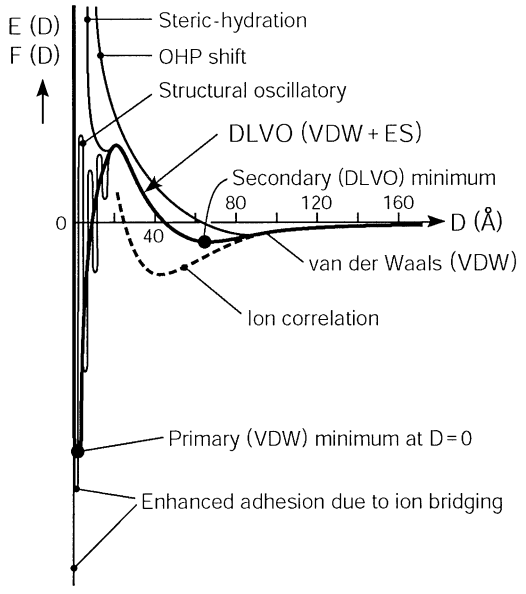

Fig. 3. Different types of short-range DLVO and non-DLVO forces *F(D)* or energies *E(D)* $-\int$-d*F*/d*D* that can arise between clay surfaces encountered in this study. DLVO (Derjaguin-Landau- Verwey-Overbeek), VDW (van der Waals), ES (electrostatic double-layer), and OHP (outer Helmholtz plane) are further defined and described in the text.

(V) At molecular contact ($D = 0$), the van der Waals adhesion force can be enhanced due to "ion-correlation" and "ion-bridging" effects, again most commonly observed with divalent counterions. Of course, the adhesion can also be *reduced* due to one or more of the repulsive interactions mentioned above.

Most of these interactions are known to be important in clays, giving rise to nonswelling or swelling clays. Clay swelling can be continuous (full swelling) or limited (crystalline swelling) depending on whether the short-range forces are monotonically repulsive or oscillatory (van Olphen, 1977; Caffrey and Bilderback, 1983; Viani et al., 1983; Kjellander et al., 1988).

Unfortunately, little systematic or detailed work has been done on these short-range forces, either experimentally or theoretically. This is because it is difficult to measure and distinguish between the many different types of interactions that can arise at short range, below 20–50 Å. However, this is precisely the sort of information that is required for gaining a deeper understanding of pressure solution mechanisms and clay surface interactions in general.

The SFA technique has also been used to measure dynamic interactions, such as the viscosities of liquids, including water, in molecularly thin liquid films. Thus, the viscosities of pure water and salt solutions have been found to be essentially the same as the bulk value for films as thin as 20 Å between both mica–mica and (amorphous) silica–silica surfaces (Israelachvili, 1986; Horn et al., 1989). However, the viscosity rises sharply as the film thickness decreases below the range of the oscillatory or monotonically repulsive structural forces of 10–15 Å, and for films only one water molecule thick between two mica surfaces, tribological measurements have found that the effective viscosity is ~4 orders of magnitude higher than

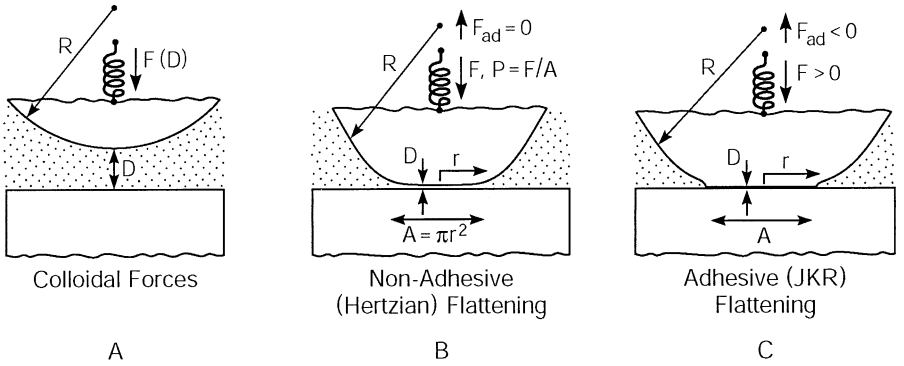

Fig. 4. Schematic of surface forces apparatus (SFA), showing the parameters that can be directly measured and the surface profiles that can be visualized when used with the FECO optical technique. (B) For non-adhering surfaces the adhesion force is zero, $F_{ad} = 0$, and the shape of the flattened surfaces under a given load F is given by the Hertz theory. (C) For adhering surfaces F_{ad} is finite, and the shape of flattened surfaces is given by the Johnson–Kendall–Roberts (JKR) theory which reduces to the Hertz theory when $F_{ad} = 0$ (Johnson, 1996).

the bulk value, and to be non-Newtonian (Homola et al., 1989; Drummond et al., 1998; Berman and Israelachvili, 2001).

This paper extends the earlier studies of the static and dynamic interactions between mica surfaces to higher pressures and both pure and mixed NaCl/$CaCl_2$ solutions.

2. EXPERIMENTAL AND THEORETICAL METHODS

2.1. The Surface Forces Apparatus (SFA)

An SFA (Israelachvili and Adams, 1978), which is shown schematically in Figure 4, was used in these studies. This apparatus allows for direct and accurate measurements of the force F or pressure P between two curved or flattened surfaces (of measurable radii R or flattened "contact" area A) as a function of their separation or water film thickness D. Previous SFA measurements of the forces between mica surfaces in NaCl solutions (sodium-mica) have produced results in good agreement with independent osmotic pressure measurements of montmorillonite clay swelling using x-ray scattering to measure the interlayer spacings (Christenson et al., 1987).

The SFA technique is conceptually similar to the AFM or any other mechanical force-measuring technique that employs a cantilever spring to measure forces, and a series of springs and piezoelectric crystals to control surface separations. In addition, because the surfaces are macroscopic (of local radius $R \sim 1$ cm and contact diameters $2r$ in the range 5–500 μm) an optical technique using multiple beam interference fringes (known as Fringes of Equal Chromatic Order of FECO) can be used to accurately and unambiguously measure the absolute (rather than relative) surface separation D to 1 Å or better (Heuberger et al., 2001) as well as the mean refractive index n of the liquid or solid film (of thickness D) between the surfaces (Israelachvili, 1973). By recording the changing FECO fringe pattern with time using a video camera-recording system, any changes in these parameters can be visualized and monitored in *real time* at the ångstrom-level, thereby providing direct information on such phenomena as crystal growth, changes in film thickness, refractive index and surface shape (Heuberger et al., 1997), and—as a consequence—ionic diffusion rates and changes in local stresses.

It is worth noting that since the optical technique used in SFA experiments allows the measurement of absolute thickness and refractive index changes occurring at the ångstrom (10^{-10} m) level over periods of days (1 day $\approx 10^5$ s), rates of change in surface separations, film thicknesses, adsorbed layers and other interfacial properties as slow as 10^{-15} m/s—corresponding to 1 mm per 32,000 years or 1 m per 32 million years—can be monitored in the laboratory in an experiment lasting only a few days.

2.2. Surfaces and Solutions Used

Thick sheets (blocks) of high quality ruby-clear muscovite mica (ideal formula: $KAl_2[Al,SiO_3]O_{10}[OH]_2$, purchased from S & J Imports, NY) were cleaved to produce step-free sheets of 2–3 μm uniform thickness and area ~ 1 cm^2, as previously described (Israelachvili and Adams, 1978). Two such sheets were glued to cylindrically curved silica disks of radius $R \approx 2$ cm and mounted in the SFA in the "crossed cylinder" configuration which is equivalent to a sphere of radius R approaching a flat, planar surface. Typical contact diameters during experiments varied from 1–100 μm, as described in the Results.

To mimic geologic water compositions, solutions of NaCl and $CaCl_2$ in the range 6 to 600 mM NaCl and 6 to 30 mM $CaCl_2$ were used as both pure and mixed electrolyte solutions. The pH was typically between 6 and 7, but a few measurements were also done at much lower and much higher pH. The water was sometimes purged with nitrogen gas to remove dissolved CO_2. Applied pressures P were varied from <0.1 to 50 MPa (<1 to 500 atm). All measurements were made at 21 °C.

2.3. Experimental Procedure

After mounting the surfaces into the SFA chamber, the chamber was purged with clean, dry nitrogen gas and then filled with pure, distilled water. The surfaces were then brought into contact. After establishing that the contact was adhesive and perfectly flat across the whole contact circle (no particles in the contact zone), the zero of distance, which defines $D = 0$ for the system, was recorded from the positions (wavelengths) of the

straight FECO fringes (Israelachvili, 1973). The surfaces were then separated and the electrolyte and pH were then changed in succession, each time measuring the colloidal forces between the surfaces on approach and separation, their adhesion, and accompanying surface deformations. In some cases the solution in the chamber was changed while the surfaces were kept pressed together under a large force. By monitoring the way the film thickness and contact area changed with time, it was possible to follow the rate of ion diffusion into or out of the gap, as well as establish the changing stresses around the contact junction from the changing shapes of the surfaces. In other measurements, two surfaces were allowed to remain close together for a long time (hours) to see whether crystal growth occurred and, if so, at what place within or around the contact region.

2.4. Theoretical Interpretation of Force and Diffusion Measurements

In a typical "force-run," the force F is measured as a function of surface separation D between two cylindrically curved surfaces of radius R. When the forces are weak (usually colloidal DLVO-type forces at long-range) one generally plots the results as *F/R versus D.* This enables comparison with other measurements using surfaces of different radii since all colloidal forces are theoretically expected to scale linearly with their radius R (Israelachvili, 1991). At separations below ~20 Å where significant flattening of the surfaces occurs over a (measurable) area A, one may now plot $P = F/A$ *versus D*, which gives the pressure as a function of water film thickness D. However, even in the case where there is no flattening, one may still plot P *versus* D by using the well-established "Derjaguin approximation" (Israelachvili, 1991), which relates the forces between curved and flat surfaces according to

$$F(D)/R = 2\pi E(D) \qquad for\ D \ll R, \tag{1}$$

where $F(D)$ is the force-distance function between the two curved surfaces of radius R, and where $E(D)$ is the corresponding energy-distance function between two flat (plane parallel) surfaces per unit area. The pressure at D was obtained by differentiating $E(D)$ with respect to D:

$$P(D) = dE(D)/dD. \tag{2}$$

Thus, by using the above two equations at different distance regimes it was possible to obtain plots of P *versus* D over the whole range of distance studied.

Equation 1 was also used to determine the adhesion energy E_0 per unit area from the measured adhesion or pull-off force F_{ad} needed to detach the surfaces from adhesive contact (from or close to $D = 0$):

$$E_0 = F_{ad}/2\pi R. \tag{3}$$

This equation is strictly valid for rigid surfaces or for particles that hardly deform during an interaction. It differs by a factor of 3/4 (25%) from the equation $E_0 = 2F_{ad}/3\pi R$ of the Johnson–Kendal–Roberts (JKR) theory for elastically deformed surfaces, as occurs at strongly adhering junctions. Given the large variability in the measured adhesion energies (~3 orders of magnitude) and their errors, no significant misrepresentation is introduced by using Eqn. 3 in all situations. More importantly, it is worth noting that both equations describe the adhesion of two surfaces that separate via a *peeling* process. Thus, the molecular processes occurring at the bifurcating boundary (crack tip) is what determines the measured adhesion forces.[1]

Since we use the DLVO theory as our reference theory for the colloidal forces, we also give the two basic equations of that theory. The expression for the attractive van der Waals energy per unit area between two flat *mica* surfaces interacting across aqueous electrolyte solutions may be expressed as

$$E_{VDW}(D) = -\mathcal{A}/12\pi D^2 = -2.2 \times 10^{-20}/12\pi D^2 \quad J\ m^{-2}, \tag{4}$$

where the Hamaker constant $\mathcal{A}$ for the mica–water–mica system is known to be approximately $\mathcal{A} = 2.2 \times 10^{-20}$ J (Israelachvili, 1991). By convention, surfaces in molecular contact are assigned a "cutoff" distance of $D = 0.165$–0.20 nm (Israelachvili, 1991). The corresponding expression for the repulsive electric double-layer energy per unit area between two flat surfaces interacting in a monovalent 1:1 aqueous electrolyte solution such as NaCl at 21 °C may be expressed as

$$E_{ES}(D) = 1.46 \times 10^{-11}\ \kappa \tanh^2(\psi_0/103) \quad e^{-\kappa D} \quad J\ m^{-2}, \tag{5}$$

where ψ_0 is the surface potential in mV, and κ^{-1} is the Debye length, which for 1:1 electrolyte solutions is given by

$$\kappa^{-1} = 0.304/\sqrt{M}\ \text{nm}, \tag{6}$$

where M is the ionic strength in moles/liter. Both of the above energies for two flat surfaces may be differentiated with respect to D to give the pressure P using Eqn. 2, and both are related to the measured force functions $F(D)$ between two *curved* surfaces by the "Derjaguin approximation," Eqn. 1. While the van de Waals force is not expected to depend on the solution conditions, Eqn. 5 shows that with increasing ionic strength (increasing κ) the electrostatic repulsion decays more rapidly, but the short-range repulsion *increases* in magnitude as $D \to 0$.[2] One may further note that since $\tanh(\infty) = 1$, the double-layer force saturates at some finite value even when the surface potential ψ_0 is infinite. Equation 5 assumes that ψ_0 remains constant during an interaction, i.e., that it is not a function of D and, implicitly, of the ionic strength or Debye length. In practice, double-layer interactions generally lie between the constant surface potential and constant surface charge limits, where the latter is more repulsive than the former at small separations but has no simple analytic form (Israelachvili, 1991). Previous experiments involving mica surfaces have shown that the interaction is closer to constant potential than to constant charge (Israelachvili and Adams, 1978; Pashley, 1981).

---

[1] In principle, two initially flat surfaces may separate while remaining flat and parallel at all stages of the separation, but this rarely occurs in practice, especially between elastic surfaces that separate slowly from each other. If two surfaces *were* to separate in this way, their adhesion force would be much higher than given by Eqn 3.

[2] As $D \to 0$, $e^{\kappa D} \to 1$, so that at constant ψ_0, $E_{ES}(D \to 0) \propto \kappa$ -1697- $\sqrt{M}$, which increases with increasing ionic strength, M.

Finally, the diffusion equation

$$\langle x \rangle^2 = \mathcal{D}t \tag{7}$$

was used to estimate the diffusion coefficient, $\mathcal{D}$, of ions diffusing a distance x through the thin water films over a time t, as ascertained from the changing thicknesses D and contact areas $A = \pi r^2$ of the films with time (Figure 4). Such kinetic measurements (cf. Figures 6–8) allowed us to distinguish between ionic diffusion and surface reactions following a change in the solution conditions (e.g., the ionic strength or pH). Thus, pure diffusive transport without surface binding or exchange changes the Debye length and therefore the range of the double-layer repulsion, which in turn modifies the water film thickness. Ionic reactions must come after the ions have diffused into the grain boundary and these affect the short-range hydration forces, which in turn modify the adhesion forces and contact area. When these two processes have different rates they can be easily distinguished from each other.

2.5. Surface Chemical Characterization Techniques

X-ray photoelectron spectroscopy (XPS) was used to identify the ionic and molecular species present on the surfaces or trapped between them (after experiments in which crystals were seen to grow on or between the surfaces). In this study, we were primarily interested in identifying the valence electrons of Ca and C to determine the nature of the crystals that formed at the mica–mica contacts. XPS has a sampling depth of about 10 Å (Sherwood, 1995). Also, secondary ion mass spectroscopy (SIMS) was used to corroborate the findings obtained with XPS, which confirmed the existence of Ca on the surfaces and in the nucleated crystals.

At the end of each experiment the solution was drained from the SFA chamber and the whole system was dried while the surfaces and trapped crystallites were kept in contact. After drying, the surfaces were separated and the contact region was analyzed by XPS (Figure 10, panels A and B) and SIMS (data not shown), which detected not only the elements that form mica (Si, O, Al, K), but also Ca, N, and Cl.

3. RESULTS AND ANALYSIS

3.1. Pressure-Distance Profiles

As expected from previous studies, in dilute solutions the measured force-distance profiles were in good agreement with the DLVO theory, viz. a combination of attractive van der Waals and repulsive electrostatic "double-layer" forces, as illustrated in Figure 2. But at higher NaCl concentrations, especially those above 1 mM NaCl which are in the range of geologic interest, additional repulsive "hydration" forces were measured. Hydration forces (cf. Figure 2) appear to be due to the binding of hydrated cations to negatively charged clay surfaces above some "critical hydration concentration," which depends on the type of ion, the nature of the surface and the pH (van Olphen, 1977). Apparently, before binding to the mica surface, only some of the water of hydration is removed from the cation, leaving a "partial" hydration shell around it (see Figure 11A, below) that is responsible for the hydration force between the surfaces. This conclusion is based on previous observations of a direct correlation between the strength of the hydration force and the hydration number or size of the hydrated cation in solution (Israelachvili and Pashley, 1982). In what follows, we concentrate most of our results on these high concentration, hydration force regimes, in the range 6 to 600 mM NaCl and 6 to 30 mM $CaCl_2$, as described in the Experimental section.

3.1.1. Pure NaCl solutions

Figure 5 shows the short-distance profiles between various mica surfaces in different solutions of NaCl. As can be seen from Figures 2 and 5, with increasing ionic strength above 1 mM, the hydration repulsion steadily increases until it reaches saturation between 6 and 60 mM NaCl. The decay length of the monotonic repulsion remains at ~1 nm up to pressures of ~50 MPa, which is similar to what has been previously found at lower pressures (Pashley, 1981; Christenson et al., 1987). Apparently, the monotonic repulsion has a roughly constant oscillatory component superimposed on it (cf. inset in Figure 2) that is due to water structuring or layering effects (Christenson et al., 1982; Israelachvili and Pashley, 1983; Israelachvili and Wennerström, 1996). For this reason, the oscillatory component, which gives rise to the limited "crystalline swelling" of clays, occurs only over a narrow range of solution conditions, viz. when the monotonic component is still small but large enough to lift the *maxima* of the oscillations above the zero-force ($F = 0$) axis but not yet strong enough to lift the *minima* above the $F = 0$ axis.

Also shown in Figure 5 are the theoretically expected DLVO forces (pressures) based on Eqns. 2, 4, and 5 assuming a constant surface potential of $\psi_0 = -75$ mV [from Eqn. 5 one may note that the double-layer forces are not much higher at higher values of ψ_0 since $\tanh(\infty) = 1$]. The large deviations from theory are in marked contrast to the good quantitative agreement obtained in dilute solutions, below 1 mM NaCl, as shown in Figure 2. Figure 5 also shows the swelling curves of various sodium-montmorillonite clays in 10 M NaCl solutions as reported by Viani et al. (1983). In these studies, the pressures were applied osmotically and x rays were used to measure the interlayer spacings, and the highest pressures reached were about 8 atm., so a detailed comparison between our present results on sodium-mica in more concentrated solutions and at higher pressures cannot be made. However, as noted earlier (Christenson et al., 1987), where a comparison can be made, the magnitude, range and decay of the hydration forces of Na-mica and Na-montmorillonite do appear to be very similar. The measured hydration forces are further described in Section 3.3.

3.1.2. Pure $CaCl_2$ solutions

As previously reported (Pashley and Israelachvili, 1984), calcium and other divalent cation solutions behave quite differently from sodium and other monovalent cation solutions. First, there is no strong calcium binding nor a repulsive hydration force until much higher concentrations, above 100 mM, are exceeded, presumably because of the stronger water-binding affinity of Ca^{2+} which is therefore less ready to lose its primary hydration shell in order to bind to the negative lattice sites on

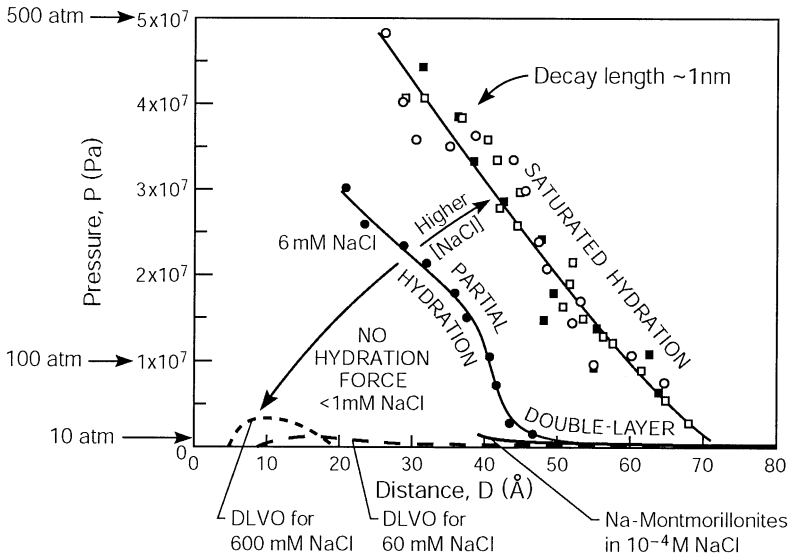

Fig. 5. Measured compressive pressures P as a function of water film thickness D under different solution conditions in pure NaCl solutions. Also shown are the theoretically expected DLVO forces based on Eqns. 2, 4, and 5 assuming a constant surface potential of −75 mV, and earlier measurements on swelling sodium–montmorillonite clays at pressures up to ~8 atm (Viani et al., 1983; Christenson et al., 1987). These results show that the hydration force due to the binding of hydrated Na^+ ions saturates between 6 and 60 mM NaCl (points ●), increasing no further between 130 and 600 mM NaCl (points ○, □, and ■, representing different experiments and force-runs).

the mica basal plane (Kekicheff et al., 1993), Second, previous force measurements on a number of different surfaces, including surfactant and lipid bilayer surfaces (Marra, 1986; Leckband and Israelachvili, 2001), suggest that short- to medium-range attractive ion correlation forces (Kjellander et al., 1988; Kekicheff et al., 1993), and calcium bridges between negatively charged surfaces in adhesive contact, enhance the attractive and adhesive forces above what is expected from the Lifshitz theory of van der Waals forces. Our present results support the existence of both of these additional attractive forces between mica surfaces, which we describe further below after we first comment on the interactions in mixed NaCl–$CaCl_2$ systems.

3.1.3. Mixed NaCl–$CaCl_2$ solutions

As might be expected, the mixed solutions behave qualitatively in between the two pure solutions, but there are quantitative subtleties arising from the competitive nature of the binding of Na and Ca ions to mica and the antagonistic effects that these ions apparently have on the contact adhesion and short-range hydration forces [similar effects are observed between biological systems (Leckband and Israelachvili, 2001)], which will now be described in turn.

3.2. Short-Range Adhesion Forces and Energies

It is instructive to first consider the theoretically expected energies and forces between two mica surfaces over the last 20 Å and especially as they approach contact in the "primary minimum" at $D = 0$. For monovalent electrolytes such as NaCl in the concentration range from 6 to 600 mM (corresponding to Debye lengths ranging from $\kappa^{-1} = 3.9$ to 0.39 nm) the surface potential is of order −75 mV at a pH of 6–7, and the Hamaker constant is $\mathcal{A} = 2.2\times10^{-20}$ J which is largely independent of the ionic conditions (Israelachvili and Adams, 1978; Pashley, 1981). With these values, one may estimate the energy (Eqns. 4 and 5) and pressure (Eqn. 2) at contact by putting $e^{-\kappa D} = 1$ for the electrostatic interaction, and an effective cutoff distance of $D_0 = 0.165$ nm for the van der Waals interaction (Israelachvili, 1991). By inserting these values into the equations, one finds that over the whole range of concentrations, both the energies and forces (pressures) at contact are negative, i.e., adhesive, because the van der Waals attraction always wins out. Thus, at 6 mM NaCl we obtain $E(0) = E_0 = -20$ mJ m^{-2} and $P(0) = -2.6 \times 10^8$ Pa, while at 600 mM we obtain $E(0) = E_0 = -7.4$ mJ m^{-2} and $P(0) = -2.2 \times 10^8$ Pa. For weaker double-layer forces the adhesion energy will be higher, up to $E_0 \sim 22$ mJ m^{-2}, while for stronger short-range electrostatic forces or for interactions at constant surface charge density rather than constant surface potential it should be weaker. Based on the above calculations, we may therefore conclude that any nonadhesive contact interaction is indicative of some non-DLVO force operating between the surfaces.

In addition, at higher ionic strengths, we expect a much weaker adhesion in the "secondary minimum" at some finite separation ranging from >100 to 20 Å. For example, in 60 mM NaCl and $\psi_0 = 75$ mV, Eqns. 4 and 5 lead us to expect $E_{min} \approx 0.005$ mJ m^{-2} at $D \approx 100$ Å.

We first describe those situations where the measured forces agree with the DLVO theory at all separations. As was previously found and illustrated in Figure 2, this occurs only in dilute monovalent solutions: below 1 mM in the case of NaCl, and below 1 M in the case of (pure) $CaCl_2$ (Israelachvili and Adams, 1978; Pashley, 1981; Pashley and Israelachvili, 1984; Kjellander et al., 1988; Israelachvili, 1991), although the strength of the adhesion in the primary minimum is well described by theory only in water and in dilute monovalent

Table 1. Adhesion energies E_0 and their equilibrium film thicknesses D_0.

Solution conditions[a]	Measured adhesion energy E_0 and separation D_0	Type of attraction or repulsion (cf. Fig. 2B)
	Pure water (<0.1 mM salt)	
Pure water	24 ± 2 mJ m^{-2} at 0-2 Å	Force-law agrees with DLVO theory at all separations. Adhesion occurs in primary minimum (at D = 0-2 Å) and agrees with (Lifshitz) theory of VDW forces[b]
	NaCl solutions	
0.1-1 mM NaCl at pH 2.7	21 mJ m^{-2} at 0-2 Å	Near zero double-layer force. Almost pure VDW force in agreement with Lifshitz theory of VDW forces[b]
0.1-1 mM NaCl, KCl and KNO_3 (previous work[c])	10 ± 3 mJ m^{-2} at 0-2 Å (in primary or first oscillatory minimum)	Structural oscillatory force with multiple adhesion minima at $D < 15$ Å. Adhesive minima and forces at $D > 20$ Å in agreement with DLVO theory
6 mM NaCl	No adhesion in primary minimum	Monotonic hydration force grows in magnitude and range. Weak adhesion in secondary minimum
60 mM NaCl	0.08 mJ/m^2 at ~70 Å (secondary minimum)	Hydration repulsion increases in magnitude and range. Weak adhesion in the secondary minimum
130-600 mM NaCl	0	Hydration repulsion saturates. No more adhesion at any separation. Corresponds to infinitely swelling clay
	$CaCl_2$ solutions	
0.1-10 mM $CaCl_2$	40-50 mJ/m^2 at 0-2 Å	
6 mM $CaCl_2$	43 mJ/m^2 at 0-2 Å	Calcium bridging and ion-correlation forces increase adhesion in primary minimum relative to sodium
30 mM $CaCl_2$	50 mJ/m^2 at 0-2 Å	
	Mixed NaCl + $CaCl_2$ solutions	
6 mM NaCl + 30 mM $CaCl_2$	26 mJ/m^2 at 18 Å	Attractive ion-correlation force increases secondary minimum, stabilized by short-range hydration repulsion

[a] pH 6-7 unless stated otherwise.
[b] Adhesion energies based on Eqn. 3: $E_0 = F_{ad}/2\pi R$. According to the DLVO theory (Eqns. 4 and 5) the adhesion energy in the primary minimum at D~0 is expected to fall approximately from 20 to 7 mJ m^{-2} with increasing NaCl concentration from 0 to 600 mM, as calculated in the text. The maximum adhesion energy in the primary minimum (D = 0-2 Å) is expected to be about 22 mJ m^{-2}.
[c] McGuiggan and Israelachvili, 1990.

solutions. Table 1 gives the measured strengths E_0 and locations D_0 of the adhesive wells (potential energy minima) as measured in both pure and mixed NaCl and $CaCl_2$ solutions.

Table 1 shows that only in pure water and in low pH conditions is the adhesion fully accounted for (both in magnitude and surface separation) by the van der Waals forces alone. At higher NaCl concentrations it is lower due to hydration effects; while in dilute $CaCl_2$ solutions it is higher due to ion-correlation forces and/or calcium cross-bridging effects, as discussed in the Introduction.

3.3. Thickness of Hydration Layers

Figure 5 shows that when pressed together at up to 500 atm, two mica surfaces cease to approach each other any closer due to the existence of some additional short-range repulsive hydration force, even though the DLVO theory predicts that the two surfaces should come into adhesive contact at $D = 0$. The hydration repulsion saturates above some ionic strength, which gives further support to the hypothesis, described in Section 3.1, that it is due to the binding of hydrated sodium ions to the mica surface. Presumably, this saturation occurs at a concentration where all (or most of) the negative sites on ion-exchanging mica surfaces have become occupied by sodium ions. At lower NaCl concentration and/or lower pH the negative surface sites are occupied by protons H^+ or hydronium ions H_3O^+ which do not give rise to a hydration force (cf. Table 1), supposedly because the protons penetrate into the mica lattice (Quirk and Pashley, 1991a).

Table 2 gives the limiting film thicknesses attained under normal pressures of 10–50 MPa (100–500 atm) under different solution conditions. These effective hard walls[3] may be considered to reflect the finite film thickness occurring between two clay surfaces (in this case of mica) through which ions can diffuse and exchange with other hydrated films or with the bulk reservoir solution.

3.4. Diffusion of Ions Through the Thin Interfacial Water Films

By *in situ* monitoring of the changing film thicknesses, contact areas and forces with time after a change in the solution conditions we could measure the rates of diffusion of ions into and out of the thin water films (and, in some cases, distinguish the diffusion from the rates of ion binding, unbinding or exchange with the surfaces). This was done by recording the changing shapes of the FECO fringes following a change of the

[3] Hard wall refers to the equilibrium water film thicknesses or surface separation distances, D, measured at normal pressures above 10 MPa (100 atm).

Table 2. Limiting water film thicknesses in NaCl, $CaCl_2$ and mixed NaCl-$CaCl_2$ solutions.

Solution conditions (at pH 6-7)	Equilibrium water film thicknesses at (lithostatic) pressures above 100 atm
	Pure water
Pure water	0–2.5 Å
	NaCl solutions
0–1 mM NaCl (previous work[a])	0–10 Å (multiple energy mimima and maxima[a])
6 mM NaCl	<20 Å
60 mM NaCl	>20 Å
130 mM NaCl	~25 Å
600 mM NaCl	~30 Å
	$CaCl_2$ solutions
0–100 mM $CaCl_2$	0–2.5 Å
>100 mM $CaCl_2$ (previous work[b])	~10 Å (possible multiple energy minima)
	Mixed NaCl + $CaCl_2$ solutions
6 mM NaCl + 30 mM $CaCl_2$	12 Å

[a] McGuiggan and Israelachvili, 1990.
[b] Pashley and Israelachvili, 1984; Quirk and Pashley, 1991; Kekicheff et al., 1993.

solution surrounding the contact junction/zone/region. Figure 6 shows the different types of experiments performed and the corresponding changes observed, and Figures 7 and 8 show results for the time evolution of NaCl-induced swelling (thickening) and $CaCl_2$-induced thinning of water films, respectively, at the low concentrations used here.

Figure 7 shows the swelling of a water film from $D = 0$–2 Å to $D = 20$ Å following the raising of the solution ionic strength from 0 to 6 mM NaCl while the surfaces were kept under a high pressure (cf. Table 2). The reduction of the contact radius r with time arises from the penetration of sodium ions into the gap (accompanied by an equal back-flow of protons to ensure charge neutrality), their binding to the surfaces, the growth of a hydration layer and force, the separation of the surfaces to 20 Å, and the elimination of the adhesion force (cf. Table 1). With the elimination of the adhesion, the contact area falls, and the boundary becomes rounded rather than sharp as the surface geometry is now described by the Hertz theory for non-adhering surfaces rather than the Johnson–Kendall–Roberts (JKR) theory for adhering surfaces (Israelachvili, 1991; Wan et al., 1992). Since the externally applied force remained constant during this swelling process, the reduction in the contact area resulted in an effective increase in the *mean* pressure at the junction, rising from $P = F/\pi r^2 = 3.2$ MPa (32 atm) at $t = 0$, to $P = 14.0$ MPa (140 atm) at $t = 14$ s when the swelling was more or less complete. However, the elimination of the adhesion alters the *local* pressure acting on the surfaces—the stress distribution within the contact area—in a subtle way: at the boundary of the junction the initially high *tensile* pressure is removed and replaced by a low *compressive* pressure. The maximum compressive pressure occurs at the center of the contact where, theoretically, it is 50% higher than the *mean* pressure (of 140 atm) (Israelachvili, 1991; Johnson, 1996).

The observed rapid penetration of hydrated sodium ions into a contact junction that is initially thinner than the diameter of a hydrated sodium ion (~4–7 Å) is consistent with previous observations of a similar effect in studies of *water* penetration into unloaded but misoriented mica sheets in (initial) dry molecular contact (Wan et al., 1992), where a diffusion coefficient of $\mathcal{D} \approx 3 \times 10^{-9}$ m^2/s was obtained. Here we find that rapid diffusion of hydrated sodium ions can occur even when the two surfaces are pressed together under a very high pressure. The surface shape changes observed during the penetration are shown schematically in Figure 6A. Applying Eqn. 7 to the results of Figure 7 gives us an estimate for the diffusion coefficient of hydrated sodium ion penetration of $\mathcal{D} \approx (20 \times 10^{-6})^2/14 \approx 3 \times 10^{-11}$ m^2/s, which is two orders of magnitude lower than the diffusion of water into mica–mica cleavage (cracks), mentioned above (Wan et al., 1992), and a factor of 40 lower than the diffusion coefficient of $\mathcal{D} \approx 1.3 \times 10^{-9}$ m^2/s of sodium ions in bulk water at infinite dilution at 25 °C (Li and Gregory, 1974).

Figure 8 shows an opposite example of a decreasing film thickness and increasing contact area following the raising of the calcium level in the NaCl solution. In further contrast to the situation with pure NaCl, the contact area remained flat throughout the "collapse" rather than having different regions change their local thickness at different times (compare Figure 6B with 6A). In addition, the transition appears to have a fast and a slow rate. We attribute the fast rate to the diffusion of calcium ions into the gap, which lowers the Debye length and thereby reduces the range of the repulsive double-layer force and increases the attractive ion-correlation force. The slower rate is most likely due to calcium binding or, more strictly, *exchange* with the previously bound sodium ions on the surface, which is presumably a much slower process. This would reduce the net negative surface charge and thereby further reduce the short-range electrostatic and/or hydration repulsion between the surfaces. In a different experiment (results not shown) the starting condition was similar to that in Figure 8 but now the pH of the solution was lowered. This resulted in an immediate (<10 s) coming together and strong adhesion of the surfaces, again indicating the rapid diffusion and, in this case, exchange of protons with the surface bound sodium ions.

Again, applying Eqn. 7 to the results of Figure 8, we obtain two diffusion coefficients, a fast one of $\mathcal{D} = 4 \times 10$–$10^{-10}$ m^2/s, presumably due to pure ion diffusion, and a slow one of $\mathcal{D} \approx 6 \times 10^{-12}$ m^2/s due to ion binding/exchange. The measured diffusion coefficient of calcium in water at infinite dilution is $\mathcal{D} = 8 \times 10$–$10$ m^2/s at 25 °C (Li and Gregory, 1974), which shows that calcium is diffusing into the narrow gap of structured water at a rate that is only a factor of 2 slower than its diffusion in bulk water. However, the rate of ion binding or exchange is much slower. We discuss the implications of these results in the Discussion section.

3.5. Crystal Growth On and Between Mica Surfaces

Under certain conditions, but only in the presence of calcium, small crystallites could be seen to grow, either at the edges or within a contact junction (see Figure 6D). Typically, these would nucleate or precipitate quickly (seconds to minutes), then grow much more slowly (days). It was not possible

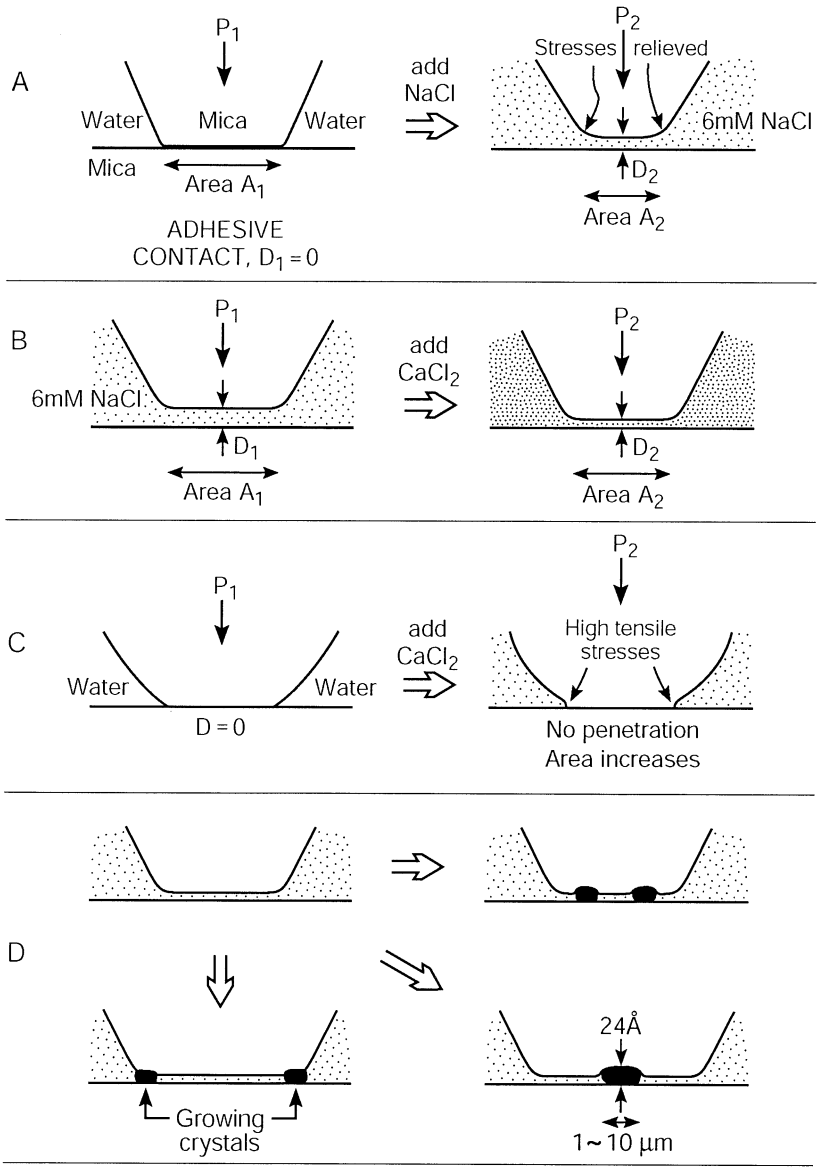

Fig. 6. Various surface shape changes, described in the text, of contact junctions following changes in the solution conditions as determined from the changing shapes and wavelengths of the FECO fringes with time. Effects that were measured (recorded) as a function of time included the film thickness D and its refractive index n, the contact radius r and area $A = \pi r^2$, the adhesion or long-range forces, the shape and sharpness of the contact boundary (which gives direct information on the stresses and strains at different locations of the junction), and crystal growth, as in panel D.

to establish what triggers the nucleation: in some cases crystallites could be seen to grow almost immediately after two surfaces were brought into contact. In other cases they appeared after two surfaces had been left in contact overnight. Figure 9A shows a FECO fringe pattern of an initially totally flat contact junction in adhesive contact in air or dilute monovalent salt solution. Figure 9B shows the FECO pattern in a solution of 30 mM NaCl + 6 mM $CaCl_2$ after a 24 Å-high crystallite had slowly grown inside the junction within 2 hours after calcium ions were introduced into the solution. Figure 9C shows a similar growth occurring just inside a boundary. It was also observed that the crystallites could move laterally within the junctions.

The growth of crystals on *isolated* mica surfaces (in contrast to their growth between two closely apposed surfaces) was not observed so long as there was no precipitation of crystals in the bulk solution (presumably, because the solubility product for the reaction $Ca^{2+} + CO_3^{2-} = CaCO_3$ was below the equilibrium constant of $10^{-8.35}$ at STP). Thus, crystals only formed *after* two surfaces had been brought into contact, or close to contact, but were never seen to be already present when two surfaces were brought together for the first time. On the other hand, if the pH of the solution in the SFA chamber was raised to above 10, rapid precipitation occurred both on the surfaces and in the bulk solution. Once grown, the crystals did not disappear but they could be moved by inducing lateral pressure

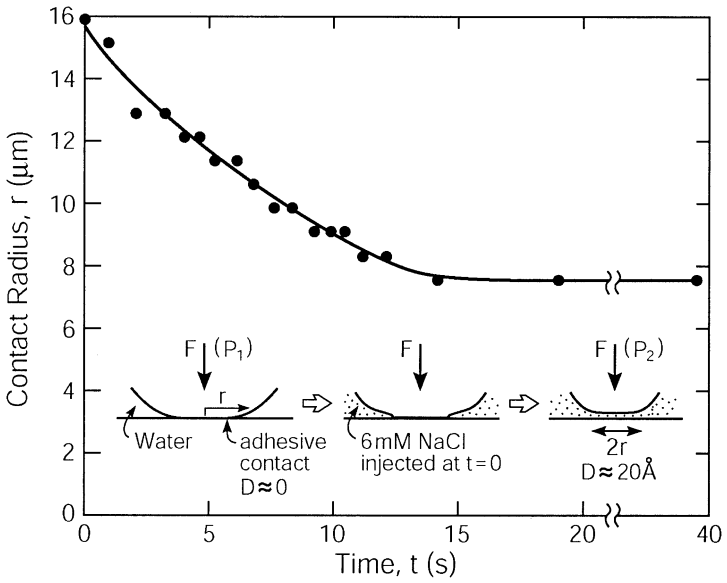

Fig. 7. Contact radius r as a function of time t after raising the ionic strength from 0 (when the surfaces are in adhesive contact) to 6 mM NaCl. The reduction in the contact radius was accompanied by the elimination of the adhesion and an increase in the films thickness from ~2 to ~20 Å (as measured at the center and shown schematically in Fig. 6(A)). Due to the constant force applied during the penetration, accompanied by the reduced radius r and area of the contact zone, the pressure increases, in this case from $P_1 = 32$ bar to $P_2 = 40$ bar (initially, in pure water, the surfaces came into adhesive contact at $D = 0$–2 Å under no external force; however, an additional external force or pressure P_1 was applied before NaCl was introduced into the solution).

gradients at the mica–mica interface, for example, during a loading–unloading cycle. To put Figures 9B, 9C, and 6D into perspective, Figure 9D, shows the common geologic occurrence of a calcium carbonate mineral crystal formed between two mica cleavage planes.

We are currently studying the physical and chemical characteristics of these crystals, such as their detailed structure, composition and growth kinetics. Our XPS and SIMS results (Figure 10) clearly show the presence of calcium and carbonate ions inside the contact junctions in which crystallites had grown, but other compounds were also detected such as CaO, CO, C, O, N (probably from the acid HNO_3), and K^+, but no

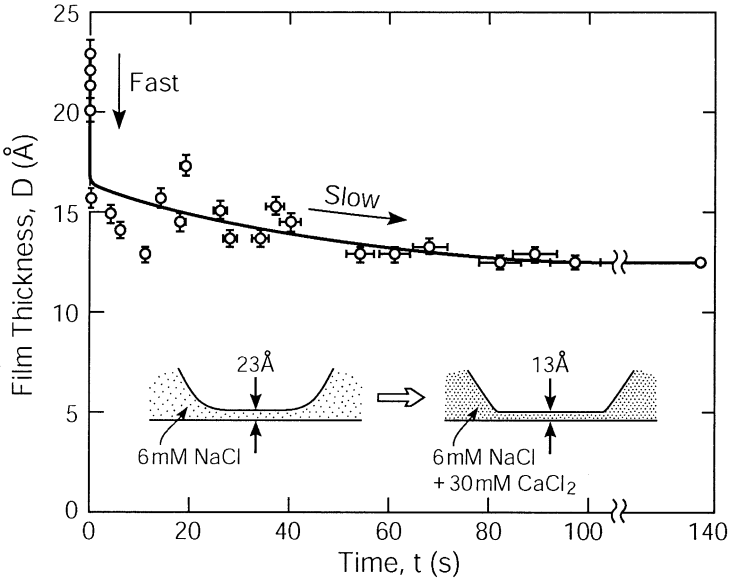

Fig. 8. Water film thickness D as a function of time t after the introduction of a 30 mM $CaCl_2$ solution into a 6 mM NaCl solution. Here, in contrast to the case shown in Figure 7, the film thickness (which was here finite at $t = 0$) *decreased* and the contact radius *increased* (slightly) with time due to the increased double-layer and ion-correlation attractive forces, as shown schematically in Figure 6(B).

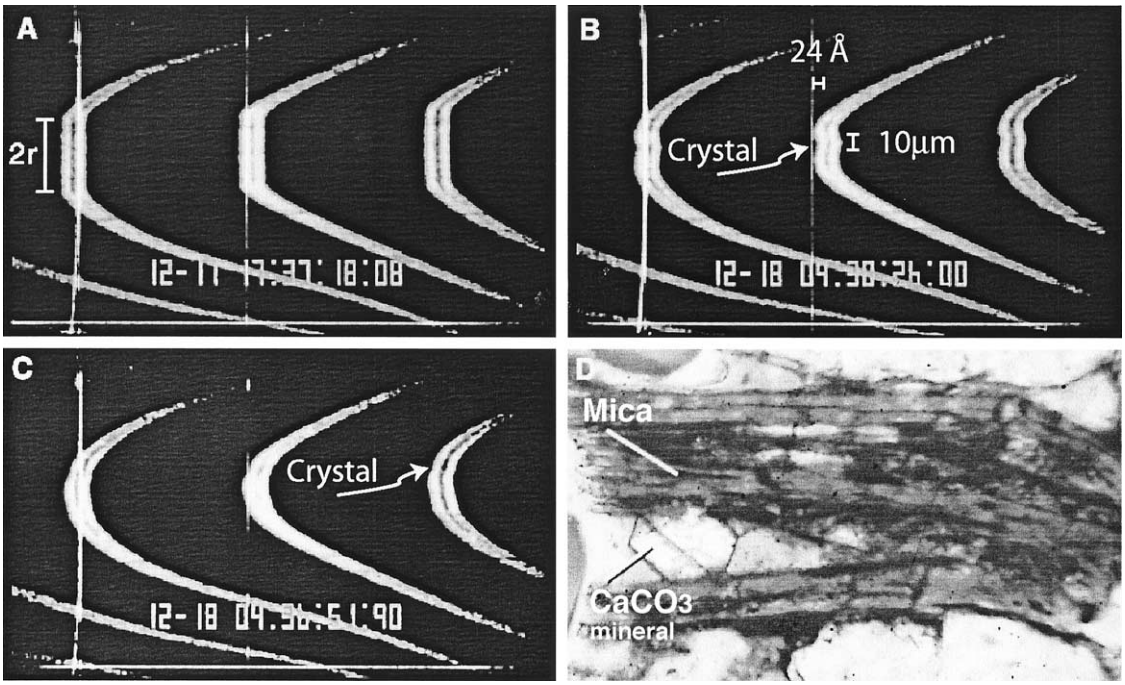

Fig. 9. FECO fringe pattern corresponding to some of the geometries depicted in Figure 6D, showing crystal growth in a solution of 30 mM NaCl + 6 mM $CaCl_2$. (A) Adhesive contact in air and in pure water or dilute monovalent salt solution. (B) A 24 Å high and ~ 10 μm wide crystal of refractive index 1.5±0.1 that had grown inside the contact area between two mica surfaces over a period of 2 hours after $CaCl_2$ was introduced into the solution. The crystal lateral dimension was about 5–10 μm typically (determined by SEM). (C) Crystal growing just inside the boundary of a contact junction within 15 minutes of calcium injection. (D) Photomicrograph of preferential growth of calcium carbonate mineral between two mica cleavage planes. Sample from Miocene sandstone at 2700 m depth, North Coles Levee oil field, San Joaquin basin, California.

Na^+. Our FECO measurements show that the crystals have a refractive index of 1.5 ± 0.1, which could include calcite or aragonite which have a refractive index of 1.49–1.68, but our measuring error with such thin crystals is too high at present to allow us to exclude other possibilities.

4. DISCUSSION AND CONCLUSIONS

A number of novel conclusions can be drawn from our studies that may also apply to other clay-mineral surfaces.

4.1. Effects of Electrolyte on Hydration and Other Short-Range Forces

Sodium and calcium have antagonistic effects (as mentioned above) on the adhesion forces, attractive electrostatic forces, and repulsive short-range hydration forces, as mentioned above and summarized in Tables 1 and 2. These, and the additional effects of pH on the surface charge and hydration, and solvent-structural forces, make each system and the solution conditions highly complex and specific, resulting in very different force-distance or pressure-distance profiles under different conditions. The range of equilibrium water gap thicknesses we find for lithostatic pressures up to 50 MPa (500 atm) range from 0 (or about one layer of water molecules) to ~30 Å, and yet, as discussed immediately below, this confinement still allows for the almost free diffusion and exchange of ions and water into and out of these gaps.

Another effect that was observed but not studied in detail was the changing shape of the junction arising from a change in the solution conditions. Thus, when calcium is added to a pure water solution, the increased adhesion (cf. Table 1) also results in a sharpening of the boundary where the surfaces bifurcate, as shown schematically in Figure 6C. This induces high negative (tensile) stresses at these boundaries that are likely to have both physical and chemical consequences.

4.2. Mobility (Diffusivity) of Ions and Water through Molecularly Thin Structured Water Films

An ultrathin water film between two surfaces, whether the water is "structured" or not, does not prevent the diffusion of water or ions into or out of the film. Even a hydrated ion such as Na^+ was found to rapidly enter into a film that is initially thinner than the hydrated diameter of the ion (cf. Figure 7); and the even more hydrated calcium ion can still enter into a highly structured water film (cf. Figure 8) with a diffusion coefficient that is not very different from its value in bulk water. Thus the idea that structured water at or between two surfaces can lower the diffusivity by many orders of magnitude is not supported by our direct measurements, at least between two mica surfaces. Compared to the diffusion coefficients of the common cations and anions in bulk water, which fall in the range 0.5×10^{-9}–2.0×10^{-9} m^2/s (Li and Gregory, 1974) (protons and hydroxide ions diffuse much faster), our values for sodium,

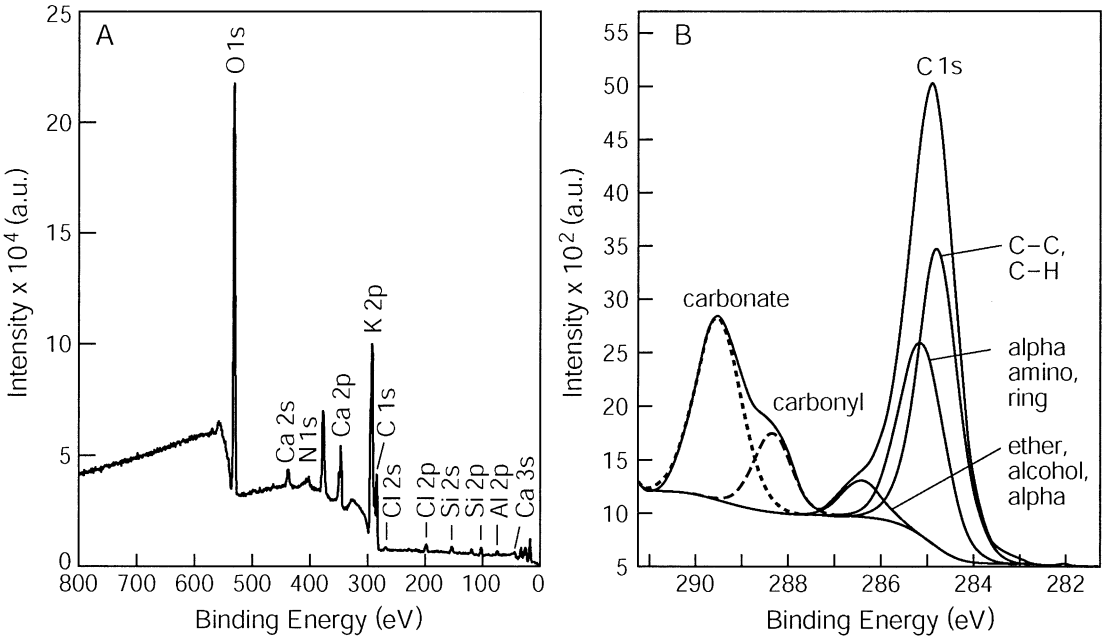

Fig. 10. XPS data on mica surfaces after an experiment in which crystallites had spontaneously grown between two surfaces while in contact in a 30 mM NaCl + 6 mM $CaCl_2$ solution at pH 6–7. The position of the Ca shown in **A** represents a binding energy of 347.2 eV, which is the binding energy of calcium carbonate (Moulder et al., 1995). Deconvolution analysis of the carbon peaks in **B** corroborate the presence of C in the carbonate and carbonyl configurations apart from the usual carbon peaks that always appear from atmospheric contaminants.

calcium, water, and protons (or hydronium H_3O^+) ions in ultrathin films fall in the range 0.4×10^{-9}–3×10^{-11} m^2/s. Thus, we conclude that the diffusivity is slowed down by two orders of magnitude at the most, and that in some cases it may not be very different from the bulk value. The same conclusion was recently reached by Revil (2001) in his analysis of electroviscous effects occurring at grain-to-grain contacts.

Significantly, for the conditions of our experiments (mica against mica, $T = 21$ °C, grain diameter ~100 μm), we find that the rate-limiting step for binding or crystal growth is not the rate at which ions reach their binding site, but the binding itself, which presumably involves an *exchange* of two hydrated species. Thus, in order to bind, the guest ion must first divest itself of its hydration shell (or part of it) while the host ion must remove itself from the surface to which it is bound. Since both ions are initially tightly bound, the first to water, the other to the surface binding site, the activation barrier for the exchange can well be imagined to be high and, therefore, rate limiting. This conclusion is consistent with some very recent measurements of ion release rates from single (unconfined) mica surfaces that found a characteristic desorption time for monovalent ions on the order of 11 minutes, corresponding to an activation energy barrier of about 33 *kT* (Raviv et al., 2002). Our results are also consistent with those of Revil's recent analysis of the kinetics of dissolution/precipitation and diffusive transport in grain-to-grain contacts, who concluded that at the temperature (~21 °C) and effective grain diameters (~100 μm) used in our experiments, pressure solution rates *should* be reaction-limited rather than diffusion-limited (see Figure 12 in Revil, 2001).

Figure 11(A) illustrates some of the different transition states or binding configurations whose energies must be considered for understanding the complex process of ion binding, exchange and crystal growth. Figure 11(A) shows how the binding sites may be (i) free, i.e., dissociated of their potassium ions and therefore negatively charged with a charge of $\frac{1}{2}e^-$, or (ii) occupied by a neutral water molecule, which has roughly the same size as potassium ions, or (iii) occupied by a partially dehydrated sodium or calcium ion, which give rise to a hydration layer and steric-hydration force, or (iv) occupied by a hydronium ion H_3O^+ where the proton H^+ is believed to be able to penetrate into the lattice (Quirk and Pashley, 1991). The binding of hydronium ions or protons to mica result in a lowering of the negative surface charge (the pK of mica is about 2) and, unlike the binding of alkali and alkali earth cations, do not give rise to an additional hydration force (cf. Tables 1 and 2). These ionic exchanges can occur when the electrolyte solution is changed (Cheng et al., 2001), or they can be triggered when two repelling surfaces are pressed together. For example, to alleviate the hydration repulsion, hydronium ions replace the surface sodium or potassium ions (Claesson et al., 1986).

The reasons for the observed high diffusivity through molecularly thin, highly structured confined liquid films may be understood from the results of computer simulations of the mobility of trapped liquid molecules in such films (Somers and Davis, 1992). Figure 11(B) is a schematic of a "structured" liquid film between two surfaces where, in spite of the structuring of the liquid into a quasi-lattice, the existence of defects allows for rapid molecular hopping to occur between occupied and unoccupied sites (vacancies), which is reflected in a high mobility (diffusion) through the highly structured interphase.

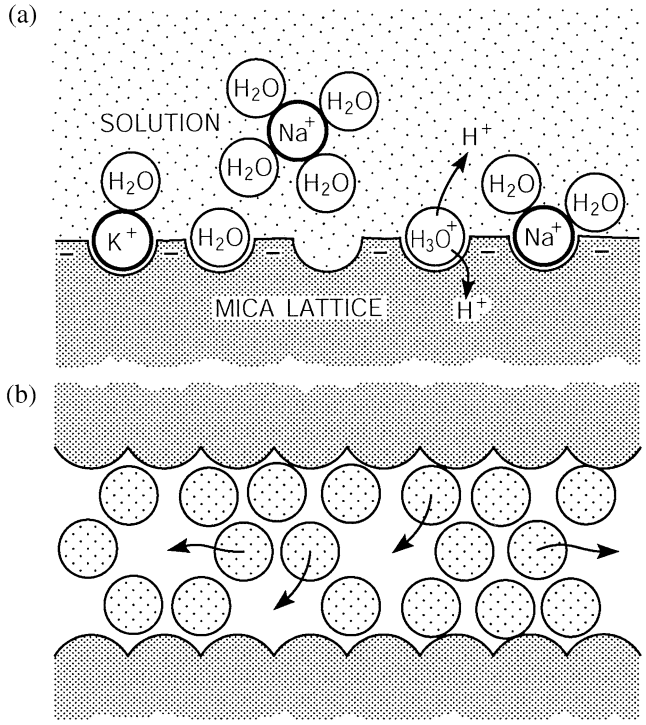

Fig. 11. (**A**) Mica basal plane exposed to aqueous electrolyte solution showing how the binding sites may be free, occupied, charged or uncharged. (**B**) Schematic of "structured" liquid film between two surfaces. (Based on a computer simulation by (Somers and Davis, 1992)).

Our results also show that by recording the changing shape, thickness and area on a contact with time following a change in the surrounding solution, it is possible to monitor and distinguish between diffusion and binding. Thus, the results shown in Figure 8 clearly indicate that diffusion occurs more rapidly than binding (or surface exchange) of ions, at least in the case of calcium exchanging with sodium or protons on the surface. Note that this ability to distinguish between different processes going on simultaneously, but at different rates, should allow for much greater insights to be obtained on the fine details of the different stages during pressure solution.

4.3. Formation and Growth of Crystals On and Between Two Closely Apposed Surfaces

The formation of crystallites between closely apposed mica surfaces was observed only in calcium solutions under conditions where such crystals do not normally form in the bulk solution. That is, they required two surfaces to nucleate them. At high pH (>10) we observed rapid precipitation even in the bulk solution, as expected, and crystallites rapidly nucleated and grew both between two closely apposed surfaces and on single, isolated surfaces. However, crystallites nucleated and grew slowly even at moderate pH and largely independent of the NaCl concentration and dissolved CO_2 so long as there was some calcium present in the solution. The XPS and SIMS data clearly show the presence of Ca^{2+} and CO_3^{2-} on surfaces that had crystallites grown between them, although other species were also present (cf. Fig. 10). The most likely candidate for these crystals is calcite ($CaCO_3$). However, they still grew in solutions that had been purged with nitrogen gas to remove dissolved CO_2, which suggests that even very low levels of dissolved CO_2 is sufficient to induce their formation or that they may be another species. Much more work has to be done on identifying the nature of these crystallites and their involvement in pressure solution, material deposition and transfer.

The growth of calcite in our experiments may be analogous to natural systems. Carbonate is commonly found between detrital mica cleavages in sandstones, typically biotite rather than muscovite. In many examples, it appears to have preferentially grown there to the exclusion of other mineral grain surfaces (Boles, 1984) and the growth has expanded the mica grain to several times its original thickness. These calcites have grown at temperatures of about 15 to 50 °C in pore fluids with abundant sodium and calcium ion and salinites near seawater values. The results of our experiments confirm that calcium carbonate crystals readily form between mica cleavages in the presence of calcium ion, even when the bulk solution is under saturated with calcite. There would appear to be several mechanisms that could cause carbonate precipitation within the mica cleavage including stripping of the hydrated water from the calcium ion allowing bonding with carbonate ion or the stripping of hydrogen ion from bicarbonate ion, freeing carbonate ion (cf. Boles and Johnson, 1984).

4.4. Implications of Results for Understanding Pressure Solution Mechanisms

Our results on mica surfaces alone do not allow us to unambiguously determine the most likely mechanism of pressure solution, for example, to favor or eliminate any one of the three major mechanisms illustrated in Figure 1. To do this, similar experiments will have to be done with quartz–quartz surfaces; and especially with *asymmetric* systems, such as quartz against mica, where we expect to see slow surface dissolution of quartz under different solution conditions and applied pressures (which does not occur with mica–mica contacts). However, if our results apply to such systems as well, and there is good reason to believe that they do, given the low, bulklike, water viscosity previously measured at silica surfaces (Horn et al., 1989), we should expect that diffusion is not always the rate-limiting step to pressure solution. Rather, the rate of ion exchange, local dissolution or crystal growth *at the dissolution or nucleation site* would be the rate-limiting step(s).

We are continuing these experiments with quartz–quartz, quartz–mica, and with biotite surfaces.

Acknowledgments—We thank Dotti McLaren for preparing the figures and Dr. Tom Mates for help with the XPS and SIMS measurements and the analysis of the data shown in Figure 10. This work was supported by NSF Grant No. EAR 0073813 and made use of the Central Facilities of the Materials Research Laboratory at UCSB which is supported by NSF Grant No. DMR96-32716.

Associate editor: D. Sverjensky

REFERENCES

Berman A. D. and Israelachvili J. N. (2001) Microtribology and microrheology of molecularly thin liquid films. In *Modern Tribology Handbook* (ed. B. Bhushan), pp. 567–615. CRC Press, Boca Raton.

Bjørkum P. A. (1996) How important is pressure in causing dissolution of quartz in sandstones? *J. Sediment Res.* **66**(1), 147–154.

Boles J. R. (1984). Secondary porosity reactions in the Stevens Sandstone, San Joaquin Valley, California. In *Clastic Diagenesis* (eds, D. A. McDonald and R. C. Surdam),Vol. 37, pp. 217–224. American Association of Petroleum Geologist.

Boles J. R. and Johnson K. S. (1984) Influence of mica surfaces on pore-water Ph. *Chem. Geol.* **43**(3-4), 303–317.

Caffrey M. B. and Bilderback D. H. (1983) Real-time X-Ray diffraction using synchrotron radiation: system characterization and applications. *Nucl. Instrum. Methods* **208**(1-3), 495–510.

Cheng L., Fenter P., Nagy K. L., Schlegel M. L., and Sturchio N. C. (2001) Molecular-scale density oscillations in water adjacent to a mica surface. *Phys. Rev. Lett.* **87**(15), 156103(4).

Christenson H. K., Horn R. G., and Israelachvili J. N. (1982) Measurement of forces due to structure in hydrocarbon liquids. *J. Colloid Interface Sci.* **88**(1), 79–88.

Christenson H. K., Israelachvili J. N., and Pashley R. M. (1987) Properties of capillary fluids at the microscopic level. *SPE Reservoir Eng.* **2**(2), 155–165.

Claesson P. M., Herder P., and Pashley R. M. (1986) An ESCA and AUGER study of ion exchange on the basal plane of mica. *J. Colloid Interface Sci.* **109,** 31–39.

Cox S. F. and Patterson M. S. (1991) Experimental dissolution-precipitation creep in quartz aggregates at high temperatures. *Geophys. Res. Lett.* **18,** 1401–1404.

den Brok S. (1998) Effect of microcracking on pressure-solution strain rate: The Gratz grain-boundary model. *Geology* **26**(10), 915–918.

Drummond C., Berman A., and Israelachvili J. N. (1998) Amontons' law at the molecular level. *Tribol. Lett.* **4,** 95–101.

Ducker W. A., Xu Z., Clarke D. R., and Israelachvili J. N. (1994) Forces between alumina surfaces in salt-solutions—Non-DLVO forces and the implications for colloidal processing. *J Am. Ceram. Soc.* **77**(2), 437–443.

Frens G. and Overbeck J. T. (1972) Repeptization and theory of electrostatic colloids. *J. Colloid Interface Sci.* **38**(2), 376–387.

Gratz A. (1991) Solution-transfer compaction of quartzites: Progress toward a rate law. *Geology* **89,** 4298–4312.

Guldbrand L., Jonsson B. O., Wennerström H., and Linse P. (1984) Electrical double layer forces. A Monte Carlo study. *J. Chem. Phys.* **80**(5), 2221–2228.

Heald M. T. (1955) Stylolites in sandstones. *J. Geol.* **63,** 101–114.

Heuberger M., Luengo G., and Israelachvili J. N. (1997) Topographic information from multiple beam interferometry in the surface forces apparatus. *Langmuir* **13**(14), 3839–3848.

Heuberger M., Zach M., and Spencer N. D. (2001) Density fluctuations under confinement: When is a fluid not a fluid? *Science* **292**(5518), 905–908.

Hochella M. F. Jr. (1995) Mineral surfaces: their characterization and their chemical, physical and reactive nature. In *Mineral Soc. Ser.,* (eds. X. Vaughan and R. A. D. Pattrick), Vol. 5 pp. 17–60. Chapman and Hall, London.

Homola A., Israelachvili J. N., Gee M., and McGuiggan P. (1989) Measurements of and relation between the adhesion and friction of two surfaces separated by thin liquid and polymer films. *J Tribol.* **111,** 675–682.

Horn R. G., Smith D. T., and Haller W. (1989) Surface forces and viscosity of water measured between silica sheets. *Chem. Phys. Lett.* **162**(4-5), 404–408.

Houseknecht D. W. (1987) Intergranular pressure solution in four quartzose sandstone. *J Sediment Petrol.* **58**(2), 228–246.

Israelachvili J. N. (1973) Thin-film studies using multiple-beam interferometry. *J Colloid Interface Sci.* **44**(2), 259–272.

Israelachvili J. N. (1986) Measurement of the viscosity of liquids in very thin-films. *J Colloid Interface Sci.* **110**(1), 263–271.

Israelachvili J. N. (1991) *Intermolecular and Surface Forces*. Academic, San Diego, CA.

Israelachvili J. N. and Adams G. E. (1978) Measurement of forces between 2 mica surfaces in aqueous-electrolyte solutions in range 0-100 nm. *J. Chem. Soc. Faraday Trans. I* **74,** 975–1001.

Israelachvili J. N. and Pashley R. M. (1982) Double-layer, van der Waals and hydration forces between surfaces in electrolyte solutions. In *Biophysics of Water* (ed. F. Franks) Wiley, New York.

Israelachvili J. N. and Pashley R. M. (1983) Molecular layering of water at surfaces and origin of repulsive hydration forces. *Nature* **306**(5940), 249–250.

Israelachvili J. N. and Wennerström H. (1996) Role of hydration and water structure in biological and colloidal interactions. *Nature (London)* **379**(6562), 219–225.

Johnson K. L. (1996) *Contact Mechanics*. Cambridge University Press, Malta.

Kekicheff P., Marcelja S., Senden T. J., and Shubin E. (1993) Charge reversal seen in electrical double layer interaction of surfaces immersed in 2:1 calcium electrolyte. *J. Chem. Phys.* **99**(8), 6098–6113.

Kjellander R., Marcelja S., Pashley R. M., and Quirk J. P. (1988) Double-layer ion correlation forces restrict calcium-clay swelling. *J. Phys. Chem.* **92**(23), 6489–6492.

Kjellander R., Marcelja S., Pashley R. M., and Quirk J. P. (1990) A theoretical and experimental study of forces between charged mica surfaces in aqueous calcium chloride solutions. *J. Chem. Phys.* **92**(7), 4399–4407.

Kruzhanov V. and Stöckhert B. (1998) On the kinetics of elementary processes of pressure solution. *Pure Appl. Geophys.* **152**(4), 667–683.

Leckband D. and Israelachvili J. N. (2001) Intermolecular forces in biology. *Q. Rev. Biophys.* **34**(2), 105–267.

Lehner F. K. (1995) A model of intergranular pressure solution in open systems. *Tectonophysics* **245,** 153–170.

Li Y. H. and Gregory S. (1974) Diffusion of ions in sea-water and in deep-sea sediments. *Geochim. Cosmochim. Acta* **38**(5), 703–714.

Marra J. (1986) Direct measurement of the interaction between phosphatidylglycerol bilayers in aqueous-electrolyte solutions. *Biophys. J.* **50**(5), 815–825.

McGuiggan P. M. and Israelachvili J. N. (1990) Adhesion and short-range forces between surfaces 2. Effects of surface lattice mismatch. *J. Mater. Res.* **5**(10), 2232–2243.

Moulder J. F., Stickle W. F., Sobol P. E., and Bomben K. D. (1995) *Handbook of X-ray Photoelectron Spectroscopy*. Physical Electronics Inc., Eden Prairie, Minnesota.

Pashley R. M. (1981) DLVO and hydration forces between mica surfaces in lithium, sodium, potassium, and cesium ions electrolyte solutions: a correlation of double-layer and hydration forces with surface cation exchange properties. *J. Colloid Interface Sci.* **83**(2), 531–546.

Pashley R. M. (1982) Hydration forces between mica surfaces in electrolyte solutions. *Adv. Colloid Interface Sci.* **16,** 57–62.

Pashley R. M. and Israelachvili J. N. (1984) DLVO and hydration forces between mica surfaces in magnesium(2+), calcium(2+), strontium(2+), and barium(2+) chloride solutions. *J. Colloid Interface Sci.* **97**(2), 446–455.

Paunov V. N. and Binks B. (1999) Analytical expression for the electrostatic disjoining pressure taking into account the excluded volume of the hydrated ions between charged interfaces in electrolyte. *Langmuir* **15,** 2015–2021.

Pittman E. D. (1974) Diagenesis of quartz in sandstones as revealed by scanning electron microscopy. *J Sediment Petrol.* **42,** 507–519.

Quirk J. P. and Pashley R. M. (1991a) The nature of "contact" in measuring the forces between muscovite surfaces. *J. Phys. Chem.* **95**(8), 3300–3301.

Quirk J. P. and Pashley R. M. (1991b) Structural component of the swelling pressure of calcium clays. *Aust. J. Soil. Res.* **29**(2), 209–214.

Quirk J. P. and Marcelja S. (1997) Application of double-layer theories to the extensive crystalline swelling of Li-montmorillonite. *Langmuir* **13**(23), 6241–6248.

Raj R. (1982) *Creep in polycrystalline aggregates by matter transport through a liquid-phase. J. Geophys. Res.* **87**(NB6), 4731–4739.

Raviv U., Laurat P., and Klein J. (2002) Time dependence of forces between mica surfaces in water and its relation to the release of surface ions. *J. Chem. Phys.* **116**(12), 5167–5172.

Renard F., Ortoleva P., and Gratier J.-P. (1997) Pressure solution in sandstones: influence of clays and dependence on temperature and stress. *Tectonophysics* **280,** 257–266.

Renard F., Park A., Ortoleva P., and Gratier J.-P. (1999) An integrated model for transitional pressure solution in sandstones. *Tectonophysics* **312,** 97–115.

Revil A. (1999) Pervasive pressure-solution transfer: a poro-visco-plastic model. *Geophys. Res. Lett.* **26**(2), 255–258.

Revil A. (2001) Pervasive pressure solution transfer in a quartz sand. *J. Geophys. Res.* **106**(B5), 8665–8686.

Rutter E. H. (1976) Kinetics of rock deformation by pressure solution. *Philos. Trans. R. Soc. London Ser. A* **283**(1312), 203–219.

Rutter E. H. (1983) Pressure solution in nature, theory and experiment. *J. Geol. Soc. London* **140,** 725–740.

Sherwood P. (1995) X-ray photoelectron spectroscopy. In *The Handbook of Surface Imaging and Visualization* (ed. A. Hubbart), pp. 875–887. CRC Press, Boca Raton.

Somers S. A. and Davis T. H. (1992) Microscopic dynamics of fluids confined between smooth and atomically structured solid surfaces. *J. Chem. Phys.* **96**(7), 5389–5407.

Spiers C. J. and Schutjens P. M. T. M. (1995) Densification of crystalline aggregates by fluid phase diffusional creep. In *Deformation Processes in Minerals, Ceramics and Rocks* (eds. D. J. Barber and P. D. Meredith), pp. 334–353. Unwin Hyman, Boston.

Tada R., Maliva R., and Siever R. (1987) A new mechanism of pressure solution in porous quartzone sandstone. *Geochim. Cosmochim. Acta* **51,** 2295–2301.

van Olphen H. (1977) *An Introduction to Clay Colloid Chemistry*. Wiley, New York.

Verwey E. J. W. and Overbeek J. T. G. (1948) *The Theory of the Stability of Lyophobic Colloids*. Elsevier, Amsterdam.

Viani B. E., Low P. F., and Roth C. B. (1983) Direct measurement of the relation between interlayer force and interlayer distance in the swelling of montmorillonite. *J. Colloid Interface Sci.* **96**(1), 229–244.

Vigil G., Xu Z., Steinberg S., and Israelachvili J. N. (1994) Interactions of silica surfaces. *J Colloid Interface Sci.* **165**(2), 367–385.

Wan K. T., Lawn B. R., and Horn R. G. (1992) Repulsive interaction between coplanar cracks in the double-cantilever geometry. *J. Mater. Res.* **7**(6), 1584–1588.

Welton J. E. (1984) SEM Petrology Atlas. Methods in Exploration series. Tulsa, Oklahoma, American Association of Petroleum Geologists, 237 p.

Weyl P. K. (1959) Pressure solution and the force of crystallization—a phenomenological theory. *J. Geophys. Res.* **64,** 2001–2025.